Journal of Solid State Chemistry 188 (2012) 26–31

Contents lists available at SciVerse ScienceDirect

Journal of Solid State Chemistry

journal homepage: www.elsevier.com/locate/jssc

Synthesis, structures and properties of the new lithium cobalt(II) phosphate $Li_4Co(PO_4)_2$

R. Glaum [a,*], K. Gerber [a], M. Schulz-Dobrick [b], M. Herklotz [c], F. Scheiba [c], H. Ehrenberg [c]

[a] Institut für Anorganische Chemie, Universität Bonn, Gerhard-Domagk-Straße 1, D-53121 Bonn, Germany
[b] BASF SE, GCC/PS – M300, 67056 Ludwigshafen, Germany
[c] Institute for Complex Materials, IFW Dresden, Helmholtzstraße 20, D-01069 Dresden, Germany

ARTICLE INFO

Article history:
Received 22 September 2011
Received in revised form
23 January 2012
Accepted 24 January 2012
Available online 2 February 2012

Keywords:
Cathode material
Intercalation compound
Solid-state reaction
Thermal analysis
UV/vis spectroscopy
X-ray diffraction

ABSTRACT

α-$Li_4Co(PO_4)_2$ has been synthesized and crystallized by solid-state reactions. The new phosphate crystallizes in the monoclinic system ($P2_1/a$, $Z=4$, $a=8.117(3)$ Å, $b=10.303(8)$ Å, $c=8.118(8)$ Å, $\beta=104.36(8)$ Å) and is isotypic to α-$Li_4Zn(PO_4)_2$. The structure of α-$Li_4Co(PO_4)_2$ has been determined from single-crystal X-ray diffraction data {$R_1=0.040$, $wR_2=0.135$, 2278 unique reflections with $F_o > 4\sigma(F_o)$}. The crystal structure, which might be regarded as a superstructure of the wurtzite structure type, is build of layers of regular CoO_4, PO_4 and LiO_4 tetrahedra. Lithium atoms Li2, Li3 and Li4 are located between these layers. Thermal investigations by *in-situ* XRPD, DTA/TG and quenching experiments suggest decomposition followed by formation and phase transformation of $Li_4Co(PO_4)_2$:

$$\alpha\text{-}Li_4Co(PO_4)_2 \xrightarrow{442\ ^\circ C} \beta\text{-}Li_3PO_4 + LiCoPO_4 \overset{773\ ^\circ C}{\rightleftharpoons} \beta\text{-}Li_4Co(PO_4)_2 \xrightarrow{quenching\ to\ 25\ ^\circ C} \alpha\text{-}Li_4Co(PO_4)_2$$

According to HT-XRPD at $\vartheta = 850\ ^\circ C$ β-$Li_4Co(PO_4)_2$ (*Pnma*, $Z=2$, 10.3341(8) Å, $b=6.5829(5)$ Å, $c=5.0428(3)$ Å) is isostructural to γ-Li_3PO_4. The powder reflectance spectrum of α-$Li_4Co(PO_4)_2$ shows the typical absorption bands for the tetrahedral chromophore [$Co^{II}O_4$].

1. Introduction

Recent decades showed an increased scientific interest in the solid-state chemistry of transition-metal open-framework compounds in particular of transition metal phosphates [1,2]. The high attention paid to this class of compounds results from remarkable chemical and physical properties and potential applications as functional materials like catalysts [3] or energy storage materials [4,5]. Since the discovery of the electrochemical properties of the olivine-type phases Li*M*PO_4 (*M*=Mn [6], Fe [7], Co [8], Ni [9]) research on synthesis of phosphates of manganese, iron, cobalt and nickel was further intensified. These works aimed especially at compounds which allow reversible deintercalation of more than only one lithium equivalent per formula. The title compound α-$Li_4Co(PO_4)_2$ is isotypic to α-$Li_4Zn(PO_4)_2$ discovered by Sandomirskii et al. [10]. The tetrahedral coordination of cobalt in polynary phosphates is rather unusual. For most ternary and polynary phosphates of cobalt(II) referenced in ICSD [11] octahedral coordination is prevailing with only few exceptions (e.g. [$Co^{II}O_4$] in $Na_2CoP_2O_7$ [12–14]).

Due to the high lithium content of α-$Li_4Co(PO_4)_2$ and the expectation that oxidation of cobalt(II) to higher oxidation states (e.g. Co^{4+} as in Li_8CoO_6 [15] and A_2CoF_6, *A*=Rb, Cs [16]) might be possible, we undertook a more detailed study into the chemical, electrochemical, structural and thermal properties of $Li_4Co(PO_4)_2$. The results are reported in this paper.

2. Experimental

2.1. Synthesis

Crystalline $Li_4Co(PO_4)_2$ has been obtained according to Eq. (1) by isothermal heating of stoichiometric mixtures of $Li_4P_2O_7$ and CoO in sealed silica tubes (72 h, 850 °C) followed by rapid quenching in cold water to ambient temperature.

$$Li_4P_2O_7 + CoO \rightarrow Li_4Co(PO_4)_2 \quad (1)$$

The starting materials in equimolar ratio were finely ground in an agate mortar and pressed into a rod-shaped pellet (130 mg). The pellet and 6 mg of iodine as mineralizer were loaded into a silica tube, sealed under vacuum and placed in a one-zone tubular furnace at 850 °C. After three days the tube was quenched to

* Corresponding author. Fax: +49 228/73 56 60.
E-mail address: rglaum@uni-bonn.de (R. Glaum).

0022-4596/$ - see front matter © 2012 Elsevier Inc. All rights reserved.
doi:10.1016/j.jssc.2012.01.054

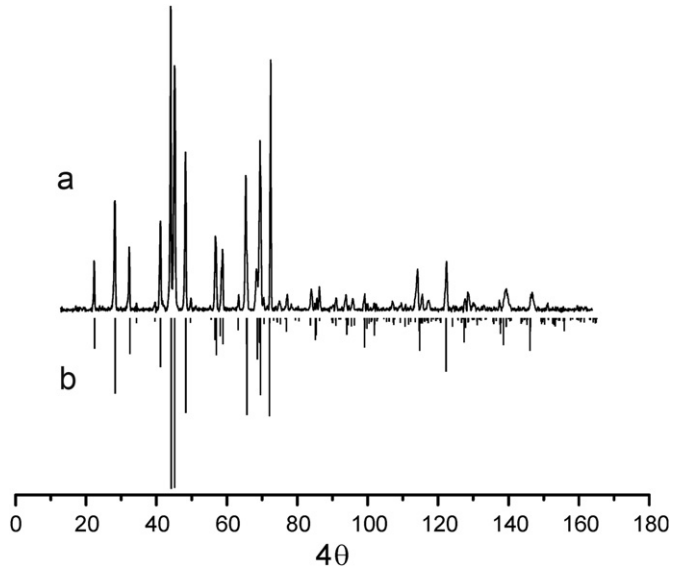

Fig. 1. Guinier photograph (Cu-$K\alpha_1$) of α-$Li_4Co(PO_4)_2$ (a) and simulated diffraction pattern (b).

ambient temperature. The deep blue crystalline samples were identified as pure α-$Li_4Co(PO_4)_2$ by Guinier photographs, Fig. 1.

Polycrystalline $Li_4P_2O_7$ for the synthesis of $Li_4Co(PO_4)_2$ was prepared according to Eq. (2).

$$2Li_2CO_3 + 2(NH_4)_2HPO_4 \rightarrow Li_4P_2O_7 + 4NH_3 + 2CO_2 + 2H_2O \quad (2)$$

Li_2CO_3 (Sigma-Aldrich, Steinheim, 99%) and $(NH_4)_2HPO_4$ (Merck, Darmstadt, $\geq$99%) were dissolved in 5 M nitric acid (Merck, Darmstadt, 65%). The solvent was slowly evaporated to dryness by constant stirring ($\vartheta_{max} \approx 200$ °C). The white residue was carefully ground in an agate mortar and heated in a silica crucible at 300 °C for 24 h. The final calcination was carried out at 600 °C in air and finished after 72 h. Powdered samples were identified as pure $Li_4P_7O_7$ [17] by Guinier photographs.

Cobalt(II) oxide was obtained by isothermal annealing of commercially available black "CoO" (Sigma Aldrich, 99.9%) which is partially contaminated by spinel Co_3O_4 [18]. The heat treatment was carried out in a silica crucible at 1100 °C in air. After 24 h the crucible was quenched to ambient temperature. The color of the oxide had changed from black to dark olive green. Thus obtained cobalt(II) oxide was free of Co_3O_4 according to Guinier photographs.

Polycrystalline α-$Li_4Co(PO_4)_2$ could also be prepared in air according to Eq. (3). Li_2CO_3 (Sigma-Aldrich, 99%), $(NH_4)_2HPO_4$ (Merck, Darmstadt, $\geq$99%) and cobalt powder (Sigma-Aldrich, 99.99%) were dissolved in 5 M nitric acid (Merck, Darmstadt, 65%). After evaporating the solution to dryness ($\vartheta_{max} \approx 200$ °C) the amorphous, purple residue was carefully ground and heated in a silica crucible at 300 °C in air for 24 h. Eventually, the material was heated at 850 °C in air for three days followed by quenching to ambient temperature. Thus obtained deep blue, crystalline samples were also single-phase α-$Li_4Co(PO_4)_2$ according to Guinier photographs.

$$2Li_2CO_3 + 2(NH_4)_2HPO_4 + Co \rightarrow Li_4Co(PO_4)_2 + 4NH_3 + 2CO_2 + 2H_2O + H_2 \quad (3)$$

2.2. Redox behavior

In order to check if the title compound shows any kind of redox activity a few milligrams (50 mg) of it were brought into contact with hydrogen peroxide. Thus, intense evolution of oxygen was observed and the color of the deep blue $Li_4Co(PO_4)_2$ lightened up. However, after drying the light-blue solid was still identified as pure α-$Li_4Co(PO_4)_2$ by Guinier photographs. Thus, no evidence for significant redox activity was found.

2.3. Thermal investigations

DTA and TG (NETZSCH STA 429 simultaneous TG-DTA thermal analyzer) were carried out under argon in the range $25 \leq \vartheta \leq 1150$ °C. A sample of powdered α-$Li_4Co(PO_4)_2$ (60 mg) was placed in a corundum crucible and heated at a rate of 7 °C/min. An empty corundum crucible of equal mass was used as reference.

2.4. X-ray powder diffraction

Powder diffraction patterns for phase identification and purity control were collected using a Guinier camera (FR-552, Enraf-Nonius Inc., Cu-$K\alpha_1$ radiation, $\lambda = 1.54051$ Å) with an image plate (BAS-TR 2025 image plate film, BAS-1800 scanner, Fuji). Details on this technique were reported in [19]. The powder diffraction pattern of α-$Li_4Co(PO_4)_2$ was indexed on the basis of the isostructural α-$Li_4Zn(PO_4)_2$ [20]. All observed reflections (24 reflections with $I_{calc}/I_{calc,max} > 0.035$) could be assigned to α-$Li_4Co(PO_4)_2$. No evidence for the presence of other phases was found in the *XRPD* pattern (for more details see Supplementary Material, Table S1). The unit cell parameters of monoclinic α-$Li_4Co(PO_4)_2$ were refined using α-SiO_2 as internal standard and the programs SOS1 and SOS2 to perform the least-squares calculations [21]. Thus, the lattice parameters $a = 8.117(3)$ Å, $b = 10.303(8)$ Å, $c = 8.118(8)$ Å and $\beta = 104.36(8)°$ were obtained.

2.5. Single-crystal X-ray diffraction

Single crystal diffraction data for α-$Li_4Co(PO_4)_2$ were collected on a Nonius κ-CCD diffractometer (Enraf-Nonius Inc., Delft) using graphite-monochromated Mo-Kα ($\lambda = 0{,}71073$ Å) radiation. Experimental conditions are given in Table 1. The data collection was performed using a blue isometric crystal with edge lengths $0.1 \times 0.15 \times 0.15$ mm^3.

A first assignment of the observed single crystal diffraction data led to an orthorhombic unit cell ($a = 9.8842(8)$ Å, $b = 12.893(1)$ Å and $c = 10.2828(8)$ Å) with systematic extinctions suggesting space group $C222_1$ (no. 20). Structure determination on the basis of this cell failed.

On closer inspection of the crystals of α-$Li_4Co(PO_4)_2$ it turned out that the orthorhombic symmetry was just the result of pseudo-merohedral twinning [22] as it was already described for α-$Li_4Zn(PO_4)_2$ [20]. Twinning is obviously favored by the dimensions of the monoclinic unit cell, with *a*- and *c*-axis being almost equal. After the collected data set was transformed according to the monoclinic unit cell the structure was eventually refined in space group $P2_1/a$ using the structural data of α-$Li_4Zn(PO_4)_2$ as starting model. The twinning of the crystal was allowed during refinement by the TWIN option in the SHELX-97 suite [23] and the twin matrix (0 0 1 0 $\bar{1}$ 0 1 0 0). A volume ratio of $V_1/V_2 = 0.957$ was found for the two twin components, which corresponds to BASF = 0.489 (in SHEXL-97). The refinement was performed using SHELX-97 in the WinGX [24] framework. Further details on the refinement are given in Table 1. Atomic coordinates and anisotropic displacement parameters can be viewed in Supplementary Material, Tables S3 and S4.

2.6. Temperature dependent X-ray powder diffraction (HT-XRPD)

In situ powder diffraction data were collected using a D8 advance diffractometer with Cu-Kα radiation (Bruker) equipped with a HTK high temperature device (Anton Paar) and an energy dispersive detector (Sol-X). The powdered sample of α-$Li_4Co(PO_4)_2$ was placed

Table 1
α-$Li_4Co(PO_4)_2$ crystallographic data, information on data collection and refinement.

	α-$Li_4Co(PO_4)_2$
Empirical formula	$Li_4Co(PO_4)_2$
Formula weight	276.9
Crystal system	Monoclinic
Space group	$P2_1/a$
T (K)	293(2)
λ (Å)	0.71073
a (Å)	8.117(3)
b (Å)	10.303(8)
c (Å)	8.118(8)
β (°)	104.36(8)
V (Å^3)	657.8(1)
Z	4
D_{calc} (g cm^{-3})	2.793
μ (mm^{-1})	3.10
Crystal dimensions (mm^3)	$0.1 \times 0.15 \times 0.16$
Crystal color	Blue
F(0 0 0)	532.0
Measured refls.	7078
Independent refls.	2756
No. of parameters	137
Theta range (°)	0.998–34.972
Index ranges	$-12 \le h \le 12$ $-16 \le k \le 16$ $-8 \le l \le 13$
GOF	1.178
R_{int}	0.055
R indicies [$I > 2\sigma(I)$]: R_1	0.040
R indicies (all data): R_1, wR_2	0.053, 0.135

$R_1 = \|F_0| - |F_c\|/\Sigma|F_0|$, $F^2 > 2\sigma(F^2)$.
$w = 1/[\sigma^2(F_0^2) + (AP)^2 + BP]$, $P = (F_0^2 + 2F_0^2)/3$.

in a corundum crucible and heated in air in the range $100\,^\circ C \le \vartheta \le 900\,^\circ C$ in steps of 50° (holding time 0.5 h) and then cooled down to 100 °C at the same rate. Powder-diffraction patterns were recorded in the range $10^\circ \le 2\theta \le 45^\circ$ for each temperature. An additional XRPD was measured after the sample was annealed at 850 °C for 16 h. The powder diffraction pattern of the high-temperature phase β-$Li_4Co(PO_4)_2$ could be reasonably well indexed on the basis of an orthorhombic unit cell *Pnma* (no. 62) with the unit cell dimensions $Z=2$, $a=10.3341(8)$ Å, $b=6.5829(5)$ Å and $c=5.0428(3)$ Å) according to γ-Li_3PO_4 [25,26]. A magnified section of the powder diffraction pattern (Fig. 2) shows some reflections, which could not be assigned on the basis of the orthorhombic cell. The complete HT-XRPD of β-$Li_4Co(PO_4)_2$ and a listing of all reflections with their assignment is given as Supplementary Material, Fig. S1 and Table S2.

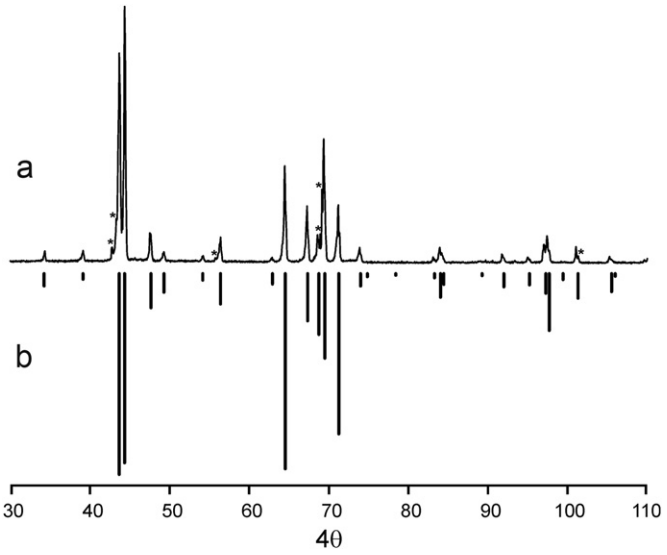

Fig. 2. HT-XRPD (850 °C; Cu-$K\alpha_1$) of β-$Li_4Co(PO_4)_2$ (a) and simulated diffraction pattern (b). Simulation based on γ-Li_3PO_4 (*Pnma* (no. 62), $Z=4$ [25,26]; cf. text) with adjusted lattice parameters: $a=10.3341(8)$ Å, $b=6.5829(5)$ Å and $c=5.0428(3)$ Å. Reflections which have not been assigned are labeled with ∗. A complete listing is given as Supplementary Material, Table S2.

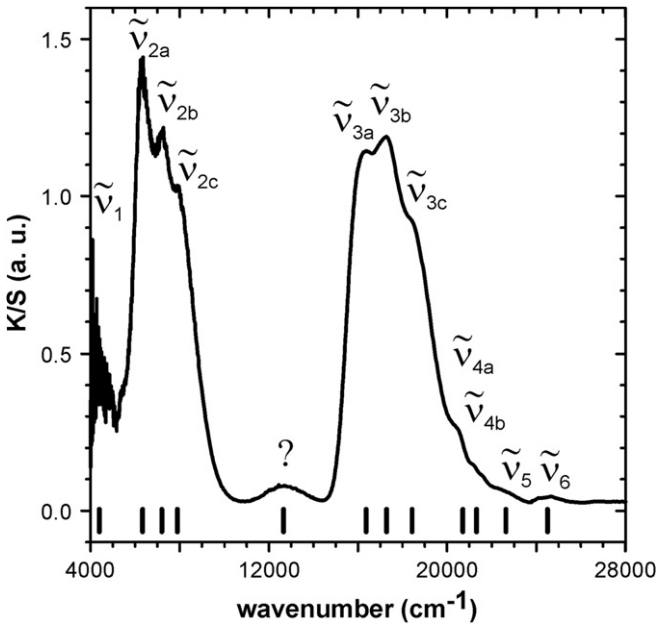

Fig. 3. UV/vis/NIR powder reflectance spectrum of α-$Li_4Co(PO_4)_2$. Ticks mark the observed transition energies.

2.7. UV–vis–NIR diffuse reflectance spectroscopy

The spectroscopic investigation ($4000 \le \tilde{\nu} \le 28000\,cm^{-1}$) was performed at ambient temperature using a modified CARY 17 spectrophotometer (OLIS Inc., USA) with a halogen lamp as light source and prism and grating as monochromator. The ratio of light scattered from sample and the reference $BaSO_4$ (Merck, Darmstadt) was measured as a function of the wavenumber $\tilde{\nu}$ (i.e. $F_{SKM}(R_\infty)$ vs. $\tilde{\nu}$ in cm^{-1}). The relation between the diffuse reflectance of the sample (R_∞), absorption (K) and scattering (S) coefficients is given by the Schuster–Kubelka–Munk (SKM) function, according to Eq. (4) [27,28].

$$F(R_\infty) = \frac{(1-R_\infty)^2}{2R_\infty} = \frac{K}{S} \quad (4)$$

Analysis of the energies of the observed electronic d–d transitions {Fig. 3; $\tilde{\nu}_1 \approx 4300\,cm^{-1}$ ($^4A_2(F) \rightarrow {}^4T_2(F)$), $\tilde{\nu}_2 = 7250\,cm^{-1}$ ($^4A_2(F) \rightarrow {}^4T_1(F)$) and $\tilde{\nu}_3 = 17270\,cm^{-1}$ ($^4A_2(F) \rightarrow {}^4T_1(P)$)} is in agreement with tetrahedral coordination of Co^{2+} in $Li_4Co(PO_4)_2$ [29,30] (Fig. 4).

By using the Tanabe-Sugano diagram [31] for d^7 systems with T_d symmetry an effective Racah parameter $B_{eff}=830\,cm^{-1}$ and the ligand-field splitting $\Delta_t=4150\,cm^{-1}$ were obtained.

2.8. Electrochemical investigations

Electrochemical experiments were carried out with a multichannel potentiostat–galvanostat (VMP 3, Bio-Logic, France). The cathode composite was prepared by mechanical mixing of 80 wt% active material with 10 wt% Super P carbon and 10 wt% polyvinylidene fluoride as polymer binder in a mortar. About 10 mg of

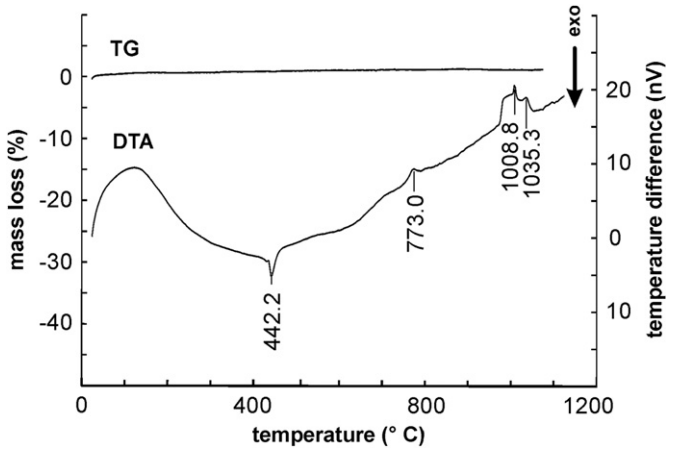

Fig.4. DTA and TG of α-$Li_4Co(PO_4)_2$.

the cathode mixture was subsequently pressed into an aluminum mesh and dried for 24 h in vacuum at 100 °C. The Swagelok-based cells were assembled in an argon-filled glove box (humidity less than 0.1 ppm water) with lithium foil as anode, 1M $LiPF_6$ in an ethylenecarbonate (EC) and dimethylcarbonate (DMC) mixture in the ratio EC:DMC=1:1 as electrolyte (NOVOLYTE, USA) and glassfiber sheet as separator. The cells were galvanostatically charged and discharged in a potential window ranging from 3 to 5 V at a C/50 rate, where 1 C was defined to be equivalent to current transferring one lithium per formula unit and hour.

Due to the metastability of α-$Li_4Co(PO_4)_2$ at ambient temperature it was impossible to obtain sufficient single phase material for electrochemical characterization. Instead all samples contained small amounts of $LiCoPO_4$ as an impurity phase. For the electrochemically analyzed sample the phase fraction of $LiCoPO_4$ could be determined by Rietveld refinement to be about 5 wt.%. Though this may be classified as a minor impurity, it turned out that this impurity complicated the interpretation of the electrochemical data significantly.

The charging curve of α-$Li_4Co(PO_4)_2$ showed two plateaus at about 4.8 and 4.9 V vs. Li/Li^+. On discharge two reduction peaks around 4.7 and 4.6 V vs. Li/Li^+ could be identified. Despite the low cycling rate only a small amount of charge was transferred in the initial cycle and only about one third of the charging capacity was retained upon discharge. The electrochemical data can be interpreted in different ways. Since the electrochemical signature resembles strongly that of $LiCoPO_4$ [32] the observed electrochemical activity might be solely due to the electrochemical reaction of the $LiCoPO_4$ impurity phase. But a decomposition of the metastable α-$Li_4Co(PO_4)_2$ into $LiCoPO_4$ and Li_3PO_4 during charge leading to electrochemically active phase $LiCoPO_4$ may be possible, too. To verify whether decomposition takes place an *ex-situ* XRD measurement of an α-$Li_4Co(PO_4)_2$ cathode recovered from a cell charged to 5 V was carried out. In the XRD pattern, no evidence for the emergence of a second phase could be observed nor could structural changes of α-$Li_4Co(PO_4)_2$ be detected. Therefore, the XRD results rather confirm the hypothesis that the electrochemical activity solely originates from the $LiCoPO_4$ impurity phase. This was further confirmed by electrochemical cycling of a $LiCoPO_4$ sample prepared under similar synthesis conditions. The charge and discharge capacity obtained for this material compared nicely to that of the α-$Li_4Co(PO_4)_2$ sample if the $LiCoPO_4$ phase in this sample was considered the only active phase.

Though α-$Li_4Co(PO_4)_2$ did not show any electrochemical activity under the electrochemical test conditions (3–5 V vs. Li/Li^+), an electrochemical activity at potentials more positive than 5 V vs. Li/Li^+ appears possible. However, electrochemical tests at such potentials are currently limited by electrolyte stability.

3. Discussion

3.1. Synthesis and thermal behavior

Crystalline $Li_4Co(PO_4)_2$ has been synthesized and characterized for the first time. Synthesis could be performed under vacuum as well as in air. Its success depends greatly on how fast the product can be quenched from the reaction temperature (850 °C) to ambient conditions. Slow cooling leads to decomposition into $LiCoPO_4$ and β-Li_3PO_4.

$Li_4Co(PO_4)_2$ as well as the isotypic $Li_4Zn(PO_4)_2$ [10,20] shows a complex thermal behavior. According to differential thermal analysis and *in-situ* XRPD α-$Li_4Co(PO_4)_2$ decomposes upon heating at approx. 442 °C by an exothermic reaction into $LiCoPO_4$ and β-Li_3PO_4 (also referred to as γ-Li_3PO_4 in a few publications [25]). At $\vartheta \approx 773$ °C these two phosphates start to react under formation of a high-temperature phase β-$Li_4Co(PO_4)_2$. No weight change is observed during these transformations. It was impossible to quench the β-phase to ambient temperature. Thus, even samples heated up to $\vartheta \approx 1100$ °C, well above the lower temperature limit of its stability range, transformed completely into α-$Li_4Co(PO_4)_2$ during quenching. Upon slow cooling (7°/h) β-$Li_4Co(PO_4)_2$ decomposes completely into $LiCoPO_4$ and β-Li_3PO_4. Obviously, at room temperature α-$Li_4Co(PO_4)_2$ has to be regarded as metastable solid. The β-phase is structurally related to γ-Li_3PO_4.

It is a quite unusual and surprising how fast formation and decomposition of $Li_4Co(PO_4)_2$ do proceed. This might be taken as indication for rather high mobility of the Li^+- and possibly even of the Co^{2+} ions. It might also point to a close structural relationship between $LiCoPO_4$ and β-Li_3PO_4 on one hand and $Li_4Co(PO_4)_2$ on the other.

3.2. UV/vis/NIR absorption spectrum

The electronic absorption spectrum observed for α-$Li_4Co(PO_4)_2$ is in agreement with the tetrahedral chromophore $[Co^{II}O_4]$. The observed ligand-field splitting $\Delta_t = 4150\,cm^{-1}$ coincides with the values found for this chromophore in other compounds (e.g., $\Delta_t(CoAl_2O_4) = 3900\,cm^{-1}$ [29,30,33] and $\Delta_t(Na_2CoP_2O_7) = 4000\,cm^{-1}$ [12,13,34]). $B_{eff} = 830\,cm^{-1}$ is expectedly lower than that of the free Co^{2+} ion ($B_{free}(Co^{2+}) = 989\,cm^{-1}$ [31]). For α-$Li_4Co(PO_4)_2$ the nephelauxetic ratio $B_{eff}/B_{free\ ion} = \beta = 0.84$ is observed. This implies some covalency in the bonding between cobalt and oxygen. The pronounced structure of the band at $\tilde{\nu}_2 = 7250\,cm^{-1}$ with components at 6280, 7200, and 7970 cm^{-1} is most likely due to splitting of the $^4T_1$ state by spin–orbit coupling. The structure of band $\tilde{\nu}_3$ might be explained by a combination of the spin-allowed transition $^4A_2(F) \rightarrow {}^4T_1(P)$ at $\tilde{\nu}_{3b} = 17270\,cm^{-1}$ and the spin-forbidden transitions to the excited states $^2E(G)$ and $^2T_1(G)$ at $\tilde{\nu}_{3a} = 16300\,cm^{-1}$ and $^2A_1(G)$ and $^2T_2(G)$ at $\tilde{\nu}_{3c} = 18470\,cm^{-1}$. The latter are gaining significant intensity by intensity stealing from the spin-allowed band due to spin–orbit coupling. Further, much weaker absorptions are observed at $\tilde{\nu}_{4a} = 20490\,cm^{-1}$, $\tilde{\nu}_{4b} = 21416\,cm^{-1}$, $\tilde{\nu}_5 = 22720\,cm^{-1}$, and $\tilde{\nu}_6 = 21416\,cm^{-1}$. In agreement with literature these can be assigned to spin-forbidden transitions to the $^2T_1(H)$ and $^2T_2(H)$, $^2E(H)$, and $^2T_1(H)$ states [30].

3.3. Crystal structure of α-$Li_4Co(PO_4)_2$

α-$Li_4Co(PO_4)_2$ is isotypic to α-$Li_4Zn(PO_4)_2$ [20]. The crystal structure can be derived from the structure of zincite (ZnO), which is usually referred to as the wurtzite type [35]. Its derivative structures are of orthorhombic (e.g. lithium orthophosphate $[Li_3P]O_4$ [29]) or monoclinic symmetry (e.g. tetralithium-cobalt-(bis)phosphate $[\square Li_4CoP_2]O_8$ [this work]). The structure can be viewed as hexagonal closest-packed

arrangement of oxygen atoms in which one-half of the tetrahedral voids is occupied by cations. The high pseudo-symmetry of the hcp anion array influences crystal growth in unfavorable ways and might lead to cation disorder and twinning.

Closer examination of the α-$Li_4Co(PO_4)_2$ structure reveals the wurtzite super structure. Its dimensions are $8\times8\times2$ of the zincite unit cell. The correlation between the unit cell of α-$Li_4Co(PO_4)_2$ and that of ZnO is specified by the transformation matrix 4.

$$8\vec{a}_w = 2\vec{b} - (\vec{a} - \vec{c})$$
$$8\vec{b}_w = 2\vec{a} - 2\vec{c}$$
$$2\vec{c}_w = \vec{a} + \vec{c} \quad (4)$$

Using this matrix allows calculation of averaged lengths for the axes of the pseudo-wurtzite subcell of α-$Li_4Co(PO_4)_2$ a_w= 3.040, b_w=3.206 and c_w=4.977. Earlier it has been shown that the ratio c/a of an ideal hcp structure is 1.633 ($=\sqrt{8/3}$) [36]. For α-$Li_4Co(PO_4)_2$, this ratio approximates $2c_w/(a_w+b_w)\approx 1.594$. This deviation from the ideal value might be one explanation for instability and decomposition of α-$Li_4Co(PO_4)_2$ upon heating.

Selected bond lengths for α-$Li_4Co(PO_4)_2$ are given as Supplementary Material, Fig. S2. Cobalt, phosphorus and lithium atoms in α-$Li_4Co(PO_4)_2$ are tetrahedrally coordinated by oxygen. Tetrahedra [CoO_4] and [PO_4] are rather regular, whereas the LiO_4-tetrahedra are somewhat distorted. On the basis of the crystal-chemical environment two types of lithium atoms can be distinguished. Atoms Li1 are part of honeycomb layers built of CoO_4-, PO_4- and $Li1O_4$-tetrahedra. Fig. 5a and b shows two different views for one of these layers. Fig. 5c visualizes the linkage of cations P^{5+}, Co^{2+} and $Li1^+$ within these layers. This view is meant to illustrate the honeycomb-like pattern of tetrahedra. Lithium atoms Li2, Li3 and Li4 are crystal chemically different compared to Li1. They are placed between the $[Li1CoP_2O_8]^{3-}$ layers. 2D mobility might be expected for them.

Along the unit cell diagonal [1 0 1] CoO_4-, PO_4- and $Li1O_4$-tetrahedra are connected to the layers and their tips are alternately ordered either up or down. This situation is well known for compounds that are derived from the wurtzite structure. This arrangement of tetrahedra has also been described for the structure of β-Li_3PO_4 where the corner-sharing LiO_4- and PO_4-tetrahedra alternating point in $+c$- or $-c$-direction [37].

3.4. High-temperature β-$Li_4Co(PO_4)_2$

The measured *in situ* powder diffraction pattern of $Li_4Co(PO_4)_2$ clearly shows formation of the high temperature phase β-$Li_4Co(PO_4)_2$. Most of the reflections of the pattern recorded at 850 °C can be assigned on basis of the orthorhombic unit cell of γ-Li_3PO_4 (*Pnma*, Z=4) [25,26]. For various distributions of Li, Co and voids on the two sites Li1 (8e) and Li2 (4c) in γ-Li_3PO_4 the XRPD pattern have been simulated. The best match (cf. Fig. 2) corresponds to full occupancy of (4c) by Li and 50% Li, 25% Co and 25% voids on (8e). Thus, even a reasonable match to the observed intensities is achieved. However, some of the reflections observed for β-$Li_4Co(PO_4)_2$ remain unindexed (e.g. 42.78°, 43.31°, 55.81°, 68.92°, 69.16°, 71.36°, and 101.34° in 4θ; Fig. 2 and Table S2). Since the additional reflections seem to arise from a splitting of reflections of the orthorhombic structure due to minor variations of edge-length and/or angles, we tried various low-symmetry distortions of the orthorhombic unit cell for assignment. Particular attention was paid to the triclinic unit cell proposed in literature for β-$Li_4Zn(PO_4)_2$ [20]. Even though we do believe that the real symmetry of β-$Li_4Co(PO_4)_2$ is lower than orthorhombic, possibly triclinic, none of our efforts led to any improved assignment of its HT-XRPD. The assignment based on β-$Li_4Zn(PO_4)_2$ still left many reflections unindexed. In addition, ambiguity in the assignment of others was found. This could not be resolved, since no atomic positions for β-$Li_4Zn(PO_4)_2$ for intensity calculations are available. In the course of these considerations, we could show that no matrix with integer determinant exists for the transformation of the unit cell proposed for β-$Li_4Zn(PO_4)_2$ to unit cells related to the Wurtzite structure family, e.g. γ-Li_3PO_4 and α-$Li_4Co(PO_4)_2$.

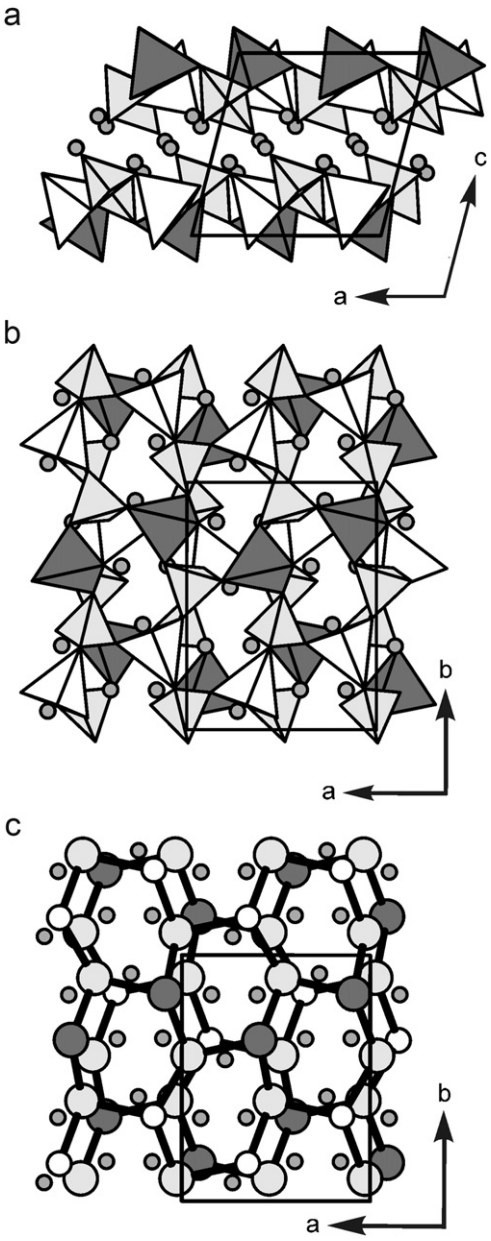

Fig. 5. Crystal structures of α-$Li_4Co(PO_4)_2$. Projections with tetrahedra PO_4: yellow, CoO_4: blue, and $Li1O_4$: gray; atoms Li2, Li3, and Li4 are shown as circles (a, b). Honey-comb network $[Li1CoP_2O_8]^{3-}$ (c), cobalt blue, phosphorus yellow, and Li1 white; oxygen atoms are omitted for clarity.

The complex thermal behavior α-$Li_4Co(PO_4)_2 \xrightarrow{442\,^\circ C}$ β-Li_3PO_4 + $LiCoPO_4 \overset{773\,^\circ C}{\rightleftharpoons}$ β-$Li_4Co(PO_4)_2$ can be described as an order–disorder transition in analogy to the transition $\beta\rightarrow\gamma$ in Li_3PO_4 [25]. However, the situation is complicated by the metastability of the α-phase with respect to its decomposition into β-Li_3PO_4 and $LiCoPO_4$. Fig. 6 presents an extract of the structure for both low- and the high-temperature phase of $Li_4Co(PO_4)_2$. While the arrangement of PO_4-tetrahedra undergoes no major

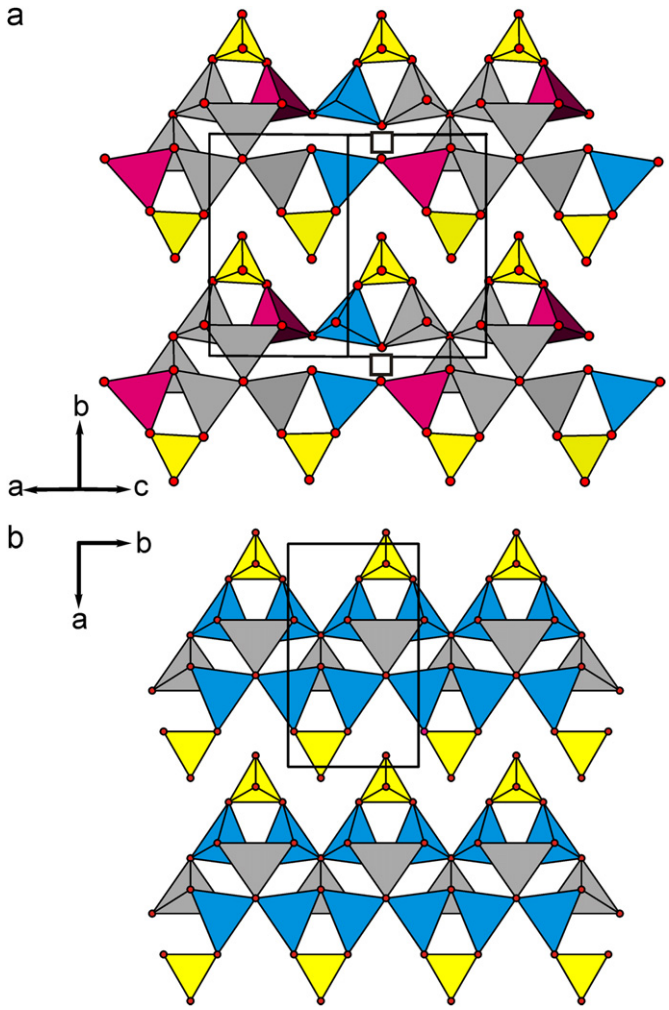

Fig. 6. Comparison of the crystal structures of α-$Li_4Co(PO_4)_2$. (a) [PO_4: yellow; CoO_4: blue; $Li1O_4$: purple; $Li2O_4$, $Li3O_4$ and $Li4O_4$:gray; tetrahedral voids are shown as squares] and the structure model of β-$Li_4Co(PO_4)_2$ [PO_4: yellow; voids, CoO_4, and $Li1O_4$: blue; $Li2O_4$: grey]. (For interpretation of the references to color in this figure legend, the reader is referred to the web version of this article.)

changes, the LiO_4- and CoO_4-tetrahedra become significantly rearranged. Higher disorder in the structure of β-$Li_4Co(PO_4)_2$ finds its expression in the mixed occupancy of the cobalt and lithium sites and disappearance of completely empty tetrahedral voids.

4. Conclusions

The α-phase of the new lithium-cobalt(II)-phosphate $Li_4Co(PO_4)_2$ has been successfully prepared by a solid-state reaction at 850 °C and subsequent quenching. Combined DTA/TG and *in situ* temperature dependant XRPD elucidate the complex thermal behavior of $Li_4Co(PO_4)_2$. Furthermore, a high-temperature phase β-$Li_4Co(PO_4)_2$ has been observed. Tetrahedral coordination for cobalt(II) in ternary and multinary phosphates is rarely observed. Surprisingly, for $LiCoPO_4$ with Wurtzite superstructure recent DFT calculations even predicted higher stability than for the actually found olivine-related structure [38]. We believe that the high Li_2O-content of $Li_4Co(PO_4)_2$ favors tetrahedral coordination of cobalt. In this sense, in agreement with our structure description (Fig. 5c), $Li_4Co(PO_4)_2$ might be regarded as lithium (lithio-cobalto-phosphate) $Li_3[LiCoP_2O_8]$.

The new material with its relatively high lithium content per cobalt atom represents an interesting candidate as cathode material for rechargeable lithium-ion batteries. While electrochemical testing showed no reversible Li^+ ion exchange up to 5 V vs. Li, possible oxidation $Co^{2+} \rightarrow Co^{4+}$ cannot be excluded so far.

Acknowledgment

We thank Dr. Gregor Schnakenburg for the collection of the single crystal X-ray data sets and staff members of the XRD-Laboratory at BASF, Germany for carrying out *in situ* XRPD measurements. This study was supported by the Germanys Federal Ministry for Research and Technology (BMBF) within the "HELION" framework.

Appendix A. Supplementary materials

Supplementary materials associated with this article can be found in the online version at doi:10.1016/j.jssc.2012.01.054.

References

[1] S. Natarajan, S. Mandal, Angew. Chem. Int. Ed. 47 (2008) 4798.
[2] A. Durif, Crystal Chemistry of Condensed Phosphates, Plenum Press, New York, 1995.
[3] J.S. Buchanan, S. Sundaresan, Appl. Catal. 26 (1986) 211.
[4] C. Batiot, B.K. Hodnett, Appl. Catal. A Gen. 137 (1996) 179.
[5] B.L. Ellis, K.T. Lee, L.F. Nazar, Chem. Mater. 22 (2010) 691.
[6] D. Wang, H. Buqa, M. Crouzet, G. Deghenghi, T. Drezen, I. Exnar, N.-H. Kwon, J.H. Miners, L. Poletto, M. Grätzel, J. Power Sources 189 (2009) 624.
[7] G.X. Wang, L. Yang, S.L. Bewlay, Y. Chen, H.K. Liu, J.H. Ahn, J. Power Sources 146 (2005) 521.
[8] M.E. Rabanal, M.C. Gutierrez, F. Garcia-Alvarado, E.C. Gonzalo, M.E. Arroyo-de Dompablo, J. Power Sources 160 (2006) 523.
[9] J. Wolfenstine., J. Allen, J. Power Sources 136 (2004) 150.
[10] P. Sandomirskii, M. Simonov, I. Belov, Dokl. Akad. Nauk. SSSR 228 (1976) 344.
[11] R. Allmann, R. Hinek, Acta Crystallogr A63 (2007) 412.
[12] L. Beaury, J. Derouet, L. Binet, F. Sanz, C. Ruiz-Valero, J. Solid State Chem. 177 (2004) 1437.
[13] F. Erragh, A. Boukhari, B. Elouadi, E.M. Holt, J. Cryst. Spect. Res 21 (1991) 321.
[14] F. Sanz, C. Parada, J.M. Rojo, C. Ruiz-Valero, R. Saez-Puche, J. Solid State Chem. 145 (1999) 604.
[15] M. Jansen, R. Hoppe, Z. Anorg. Allg. Chem. 398 (1973) 54.
[16] J.W. Quail, G.A. Rivett, Can. J. Chem. 50 (1972) 2447.
[17] O.V. Yakubovich, O.K. Mel'nikov, Kristallografiya 39 (1994) 815.
[18] R. Ross, Ph. D. thesis, University of Gießen, 1990.
[19] K. Maaß, R. Glaum, R. Gruehn, Z. Anorg. Allg. Chem. 626 (2002) 1663.
[20] T.R. Jensen, R.G. Hazell, A. Nørlund Christiansen, J.C. Hanson, J. Solid State Chem. 166 (2002) 341.
[21] J. Soose, G. Meyer, SOS—Programme zur Auswertung von Guinier-Aufnahmen, University of Gießen, 1980.
[22] P. Müller, R. Herbst-Irmer, A.L. Spek, T.R. Schneider, M.R. Sawaya, Crystal Structure Refinement: A Crystallographer's Guide to SHELXL, Oxford University Press, 2006.
[23] G.M. Sheldrick, SHELX-97 (Includes SHELXS97, SHELXL97, CIFTAB) Programs for Crystal Structure Analysis (Release 97-2), University of Göttingen, 1998.
[24] L.J. Farrugia, J. Appl. Crystallogr. 32 (1990) 837.
[25] E. Reculeau, A. Elfakir, M. Quarton, J. Solid State Chem. 79 (1989) 205.
[26] O.V. Yakubovich, V.S. Urusov, Crystallogr. Rep. 42 (1997) 261.
[27] P. Kubelka, F. Munk, Z. Technol. Phys. 12 (1931) 593.
[28] A. Schuster, Astrophys. J. 21 (1905) 1.
[29] H.A. Weakliem, J. Chem. Phys. 36 (1962) 2117.
[30] D. Reinen, Struct. Bonding 7 (1970) 114.
[31] B.N. Figgis, M.A. Hitchman, Ligand Field Theory and Its Applications, Wiley-VCH, 2000.
[32] N.N. Bramnik, K. Nikolowski, C. Baehtz, K.G. Bramnik, H. Ehrenberg, Chem. Mater. 19 (2007) 908.
[33] B. Winkler, M.J. Harris, R.S. Eccleston, K. Knorr, B. Hennion, Phys. Chem. Miner. 25 (1997) 79.
[34] P. Brinkmann, R. Glaum, Unpublished Results, University of Bonn, 2005.
[35] W.H. Bragg, W.L. Bragg, X-Rays and Crystal Structure, Bell, London, 1915.
[36] W.H. Baur, T.J. McLarnan, J. Solid State Chem. 42 (1982) 300–321.
[37] B. Wang, B.C. Chakoumakos, B.C. Sales, B.S. Kwak, J.B. Bates, J. Solid State Chem. 115 (1995) 313–323.
[38] G. Hautier, A. Jain, S.P. Ong, B. Kang, C. Moore, R. Doe, G. Ceder, Chem. Mater. 23 (2011) 3495.